Diffraction in high numerical aperture systems: polarization effects

J. Opt. **12** (2010) 015408 (6pp) doi:10.1088/2040-8978/12/1/015408

Diffraction in high numerical aperture systems: polarization effects

L Ciocci[1,2], R M Echarri[1,2,3] and J M Simon[2,3]

[1] Consejo Nacional de Investigaciones Científicas y Técnicas (CONICET), Argentina
[2] Departamento de Física, Facultad de Ingeniería, Universidad de Buenos Aires, Av. Paseo Colón 850, C1063ACV, Buenos Aires, Argentina
[3] Universidad Nacional de General Sarmiento, Argentina

E-mail: ligia.ciocci@gmail.com

Received 25 August 2009, accepted for publication 25 September 2009
Published 25 November 2009
Online at stacks.iop.org/JOpt/12/015408

Abstract
In high numerical aperture systems polarization effects should be taken into account; hence it is necessary to use a vectorial diffraction theory to describe them. We develop a computational model to study image formation in a high numerical aperture microscope objective by simulating images of self-luminous, non-polarized point objects. We compare the predictions made by scalar and vectorial theories of diffraction. In the last case we also consider an analyzer placed behind the objective to study the polarization effects. We find that vectorial theory predicts a larger diffraction pattern and, when an analyzer is used, an enlargement along the transmission axis of the analyzer. We also study the resolution of the system, finding that the true resolution predicted for vectorial theory is approximately 10% lower than that usually expected for scalar theory.

Keywords: diffraction, high numerical aperture, vectorial theory, image formation, polarization, numerical simulation

1. Introduction

In most cases diffraction of light is treated using a scalar theory, and this is accurate within the small-angle approximation. A clear example of the insufficiency of this approach is the observation of fringe inversion using a microscope. Let us consider a Lloyd interferometer studied far from grazing incidence, in which moiré fringes are used to observe contrast inversion (e.g. Simon *et al* 1987). For an incidence angle of 45° and polarization within the incidence plane, interference beams are normal to each other, as their polarizations. This implies null contrast of the interference fringes. When observed through the microscope, the directions of the beams are changed and well-contrasted fringes are seen (see figure 1). High aperture objectives may have $\sin\alpha = 0.95$ and therefore entrance angles $\alpha \sim 72°$, meaning that for certain beams there is contrast inversion of the fringes, which modifies the diffraction pattern. This suggests the need of a vectorial diffraction theory to study image formation in high numerical aperture systems.

Most previous studies on image formation in high numerical aperture systems use a theoretical approach to vectorial diffraction theory, based on the work by Richards and Wolf (1959). These authors studied the case of a linearly polarized parallel beam entering a microscope objective, assuming perfect image formation. They analyzed the diffraction pattern around the image formed at the focus and found differences between the diffraction patterns for scalar and vectorial theories.

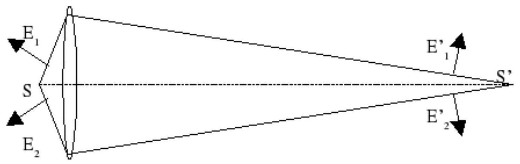

Figure 1. Contrast inversion through a microscope. S is a point source and the electric fields $\vec{E}_1$ and $\vec{E}_2$ are nearly parallel. After going through the system the fields $\vec{E}'_1$ and $\vec{E}'_2$ are almost antiparallel in the image S′. This means that interference fringes due to $\vec{E}'_1$ and $\vec{E}'_2$ in the image have inverse contrast to $\vec{E}_1$ and $\vec{E}_2$ in the object.

More recently, Sheppard and Wilson (1982) theoretically studied the image formation of a single point in a high numerical aperture microscope, finding that the central peak is broadened, the outer rings strengthened and the minima

are made shallower as the numerical aperture is increased. Török *et al* (1997) studied the properties of the polarized light and confocal microscopes considering the changes caused by using high numerical aperture objectives. Wilson *et al* (1997) analyzed the image formation in conventional and confocal polarization microscopes in the case of dielectric point scatterers. Because of its relevance to different fields of optics (e.g. focalization in high numerical aperture systems, investigation of properties in micro-optics elements and data storage, to name a few) vectorial theories of diffraction are widely employed and there are many other works on this subject. The interested reader may find a more extensive list in the review by Zhan (2009), oriented to the study of cylindrical vector beams. However, we could not find in the literature any reference to the study of image formation in conventional microscopes with analysis of polarization, nor the use of a self-luminous point object rather than a point scatterer.

In this work we study the diffraction pattern of a self-luminous, unpolarized point object seen through a high numerical aperture conventional microscope, taking into account the vectorial nature of light in the Huygens–Fresnel principle. We present a simplified fully numerical model to calculate the diffraction pattern and the optical system resolution for both scalar and vectorial theories. In section 2 we describe the theoretical basis of our model, which we present in section 3. In section 4 we analyze the resolution of the system and finally in section 5 we present our conclusions.

2. Theory and previous considerations

To study image formation through a microscope objective we make some hypotheses on the object and the optical system. We consider a self-luminous, unpolarized point object with dipolar electric moment randomly varying with time and no preferred direction in space. To calculate the time average of image intensity we model the object as a superposition of three uncorrelated orthogonal dipoles.

A high resolution microscope objective may contain 15 or more lenses, making it very difficult to follow light propagation in every surface. To simplify its treatment we do not consider here the microscope's internal structure. We assume that it is aberration-free, that it does not show birefringence nor polarization and that it satisfies the Abbe sine condition. We also consider that the system has a symmetry axis and that the point object is located on that axis. Besides, we assume that for a meridional ray, which means a ray contained in the symmetry plane, the component of the polarization vector normal to this plane is conserved.

The electric field produced by a point dipole is given by

$$\vec{E} = \frac{k^2(\hat{n} \times \vec{p}) \times \hat{n}}{r} e^{ikr}, \tag{1}$$

where $\hat{n}$ is a unit vector pointing in the direction of the ray, $\vec{p}$ the electric dipolar moment, r the distance to the electric dipole and k the wavenumber (see, e.g., Jackson 1975).

Let us consider three orthogonal point vectors $\vec{p^x}$, $\vec{p^y}$ and $\vec{p^z}$, oriented as shown in figure 2. Each dipole produces an

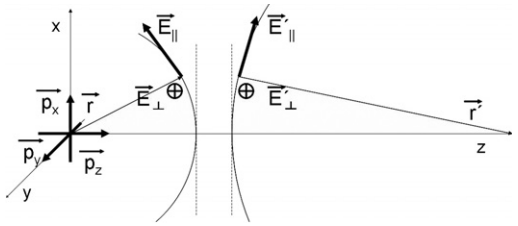

Figure 2. To simulate the object we use three orthogonal point dipoles oriented according to the coordinate axis: $\vec{p^x}$ along the x axis, $\vec{p^y}$ along the y axis and $\vec{p^z}$ along the z axis. The microscope symmetry axis is z. The action of the optical system on each component of the total electric field is projected on a reference sphere in two directions: one normal to the plane defined by the two ray vectors, $\vec{r}$ and $\vec{r'}$, and the other within this plane. The normal component $\vec{E}_{\perp}$ does not change modulus nor direction when going through the system. The parallel component of the electric vector $\vec{E}_{\perp}$ does not change direction when going through the system.

electric field given by

$$\vec{E^x} = \vec{p^x}((r_z^2 + r_y^2)\hat{x} - r_x r_y \hat{y} - r_x r_z \hat{z}), \tag{2}$$

$$\vec{E^y} = \vec{p^y}(-r_x r_y \hat{x} + (r_z^2 + r_x^2)\hat{y} - r_y r_z \hat{z}), \tag{3}$$

$$\vec{E^z} = \vec{p^z}(-r_x r_z \hat{x} - r_y r_z \hat{y} + (r_z^2 + r_y^2)\hat{z}), \tag{4}$$

where $\vec{E^x}$ is the electric field produced by the dipole $\vec{p^x}$, $\vec{E^y}$ the electric field produced by the dipole $\vec{p^y}$, $\vec{E^z}$ the electric field produced by the dipole $\vec{p^z}$, and r_x, r_y and r_z are the components of the object ray. It is important to notice that $\vec{E^x}$, $\vec{E^y}$ and $\vec{E^z}$ are not the components of the total electric field but the contributions made by the dipoles $\vec{p^x}$, $\vec{p^y}$ and $\vec{p^z}$.

We use as a reference the meridional plane defined by the object ray $\vec{r}$ and the corresponding image ray $\vec{r'}$, which also contains the symmetry axis. To match the electric fields before and after the optical system, we use two reference spheres centered one in the object and the other at its image, as shown in figure 2. The total electric field is tangential to the spheres and normal to the rays. We project this field in two orthogonal directions, one in the reference plane and the other perpendicular to that plane. The latter is characterized by the unitary vector

$$\hat{v}_{\perp} = \frac{1}{|\vec{r} \times \vec{r'}|} \vec{r} \times \vec{r'}. \tag{5}$$

We obtain the component of the electric field perpendicular to the reference plane ($\vec{E}_{\perp}$) as

$$\vec{E}_{\perp} = \vec{E} \cdot \hat{v}_{\perp} \tag{6}$$

and the component of the electric field parallel to the reference plane ($\vec{E}_{||}$) as

$$\vec{E}_{||} = \vec{E} - \vec{E}_{\perp}. \tag{7}$$

The optical system acts differently on each component. The normal component $\vec{E}_{\perp}$ does not change its modulus nor its direction when going through the system. This is valid assuming that optical surfaces have ideal antireflex treatments. Due to the axial symmetry of the system, a vector normal to the reference plane is parallel to the optical surface of the system.

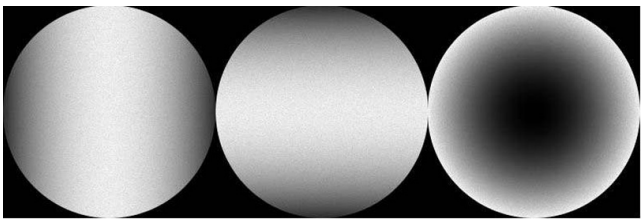

Figure 3. Electric field intensity in the entrance pupil. The left image corresponds to the amplitude of the electric field produced by the dipole oriented along the x axis (horizontal to the image), $\vec{E}^x$. The middle image corresponds to the amplitude of the electric field produced by the dipole oriented along the y axis (vertical to the image), $\vec{E}^y$. The right image corresponds to the electric field produced by the dipole oriented along the z axis, $\vec{E}^z$. In the three cases the intensity distributions are as expected.

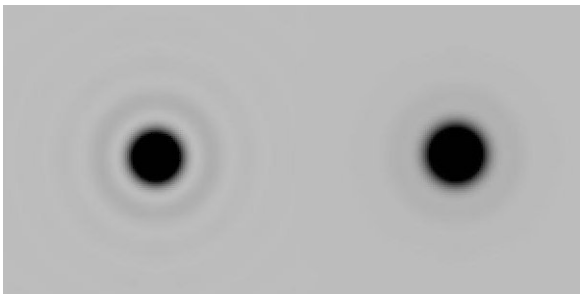

Figure 4. Simulated images of a self-luminous point object. To the left the image corresponding to scalar diffraction theory. To the right the image corresponding to vectorial diffraction theory. The radius of the diffraction pattern is larger for the vectorial theory.

The parallel component of the electric vector is continuous across an interface, therefore $\vec{E}_\perp$ is continuous. This fact can be generalized to all the surfaces in the microscope objective, and therefore to the microscope as a whole. In the same way, the parallel component $\vec{E}_{||}$ does not change its modulus, although its direction changes.

Once the electric field in the image plane is known, we calculate its contribution to each point of the image, and then the intensity for each dipole. Since the dipoles are uncorrelated, the total intensity is the sum of the contribution of each one.

The previous analysis was given for an axial point. In the case of an off-axis point if we assume a square 1 cm CCD chip, numerical aperture 1.5 and 100×, the field angle is approximately 0.03 rad. Taking the aperture stop at the image focus of the objective, we calculate the diffraction pattern on a plane normal to the principal ray. This pattern is the same as that calculated for an axial point, but in a plane rotated with respect to the plane normal to the microscope axis. The angle between these two planes is at most 0.03 rad, making the effects of the tilt negligible.

Wolf and Richards considered a polarized beam from the long conjugate that converges in the short conjugate. This leads to a correlation between the field components $\vec{E}_x$, $\vec{E}_y$ and $\vec{E}_z$ in the image. This correlation has no consequences on the image intensity distribution given that $I = |\vec{E}_x|^2 + |\vec{E}_y|^2 + |\vec{E}_z|^2$. However, when optical systems are coupled, diffraction patterns in successive images do not result in the reproduction of the former diffraction pattern with a change in the scale corresponding to the magnification. On the other hand, if we consider self-luminous, unpolarized objects, the components of the electric dipole vector $\vec{p}^x$, $\vec{p}^y$ and $\vec{p}^z$ are not correlated, and we find that, when an object is placed in the short conjugate and its image is observed in the long one, or vice versa, the diffraction patterns differ only in the magnification of the system. We have verified this property by simulating both images and comparing its intensity profiles, finding no difference between them.

3. Numerical results

We developed a numerical code, written in C, to simulate the image of a point object seen through a microscope objective for both the scalar and the vectorial diffraction theories. To simulate the image it is necessary to calculate the Kirchhoff diffraction integral, and this is done by using a numerical method that combines ray tracing and a Monte Carlo routine. We select at random an object ray and follow its path according to geometrical optics. Then we calculate the electric field in the entrance pupil and in the image plane, following this ray. Rays near the z axis ($(n_z{}^2 - 1)^{1/2} < 10^{-10}$) are not taken into account to avoid indeterminations. We use a large number of rays ($N = 10^6$) and we add the contributions to the electric field vector in the image for each ray. Knowing the total electric field at each point of the image, and the corresponding intensity, and due to the noncorrelation between the dipoles, the image is obtained by adding the intensities produced by each one of them.

As a control to our code we calculated the distribution of intensity in the exit pupil, as can be seen in figure 3. The intensities in the pupil agree with theory, as can be seen by analyzing the angular distribution of radiation for each dipole.

In figure 4, we show the images of a point source considering both the scalar and vectorial diffraction theories. It can be noticed that the radius of the diffraction pattern is larger for the vectorial theory than for the scalar case. We also introduced an analyzer behind the objective and calculate the images, in the case of vectorial theory, considering that its transmission axis can take two orthogonal directions. We show these images in figure 5. It can be noticed that the diffraction pattern is enlarged along the transmission axis of the analyzer. This effect is also present in experimental images, as can be seen in figure 6. All these images were simulated using $\sin\alpha = 0.95$.

We also obtain the intensity profiles predicted for vectorial theory by simulating the image of a single point for several values of $\sin\alpha$, and taking the intensity in vertical and horizontal lines that pass through the center of the image. In figure 7 we show the horizontal intensity profiles considering an analyzer with its transmission axis oriented along the horizontal direction in the image. It can be noticed that the radius of the central peak of the diffraction pattern is

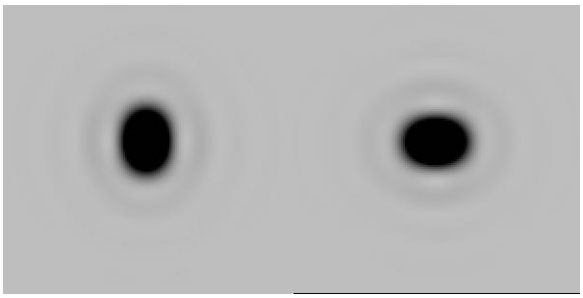

Figure 5. Simulated images of a self-luminous point object considering the vectorial diffraction theory and introducing an analyzer behind the objective. To the left the image for the transmission axis of the analyzer placed vertically to the image. To the right the image for the transmission axis of the analyzer placed horizontally to the image. In both images the diffraction pattern is enlarged along the transmission axis of the analyzer.

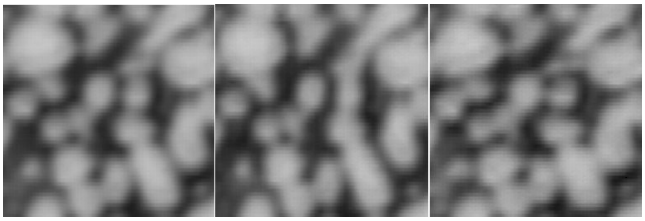

Figure 6. Episcopic images of a metallographic object. The left image is taken without an analyzer. The central image corresponds to the same object, but introducing an analyzer behind the microscope with its transmission axis along the vertical direction. The right image corresponds to the same object, but introducing an analyzer behind the microscope with its transmission axis along the horizontal direction. In this case the diffraction pattern is also enlarged along the transmission axis of the analyzer. These images were taken with a $\sin\alpha = 0.85$ dry objective.

broadened as the numerical aperture is increased, and that it is always larger than that predicted from scalar theory. In figure 8 we show the horizontal intensity profiles considering an analyzer with its transmission axis oriented along the horizontal direction in the image. It can be noticed, as in the former case, that the distance to the central peak of the diffraction pattern is broadened as the numerical aperture is increased and that it is always larger than that corresponding to the prediction from scalar theory. When both figures 7 and 8 are compared, we can see that the distance to the central peak in a vertical line is shorter in a horizontal line than in a vertical line, as we noticed in the previous images.

4. Resolution of the system

We studied the resolution of the system by simulating an image of two points separated a distance d and finding d in which the system resolution limit is achieved, and compared for scalar and vectorial diffraction theory. For $d = 19$ pixels in the image we found that for scalar theory the points are just resolved (in the resolution limit), while for vectorial theory they are not resolved, as can be seen in figure 9. When $d = 21$ pixels in the image for scalar theory the two points are well resolved,

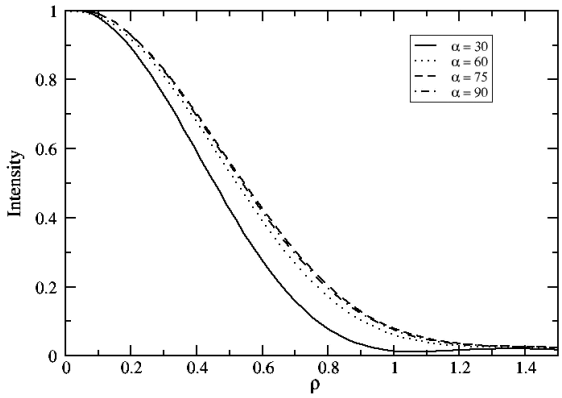

Figure 7. Intensity profile in a direction normal to that of the transmission axis of the analyzer for different numerical apertures. The intensities are normalized to unity and the distance to the center of the image is scaled by the radius of the central peak predicted for scalar theory. The radius of the central peak of the diffraction pattern is broadened as the numerical aperture is increased.

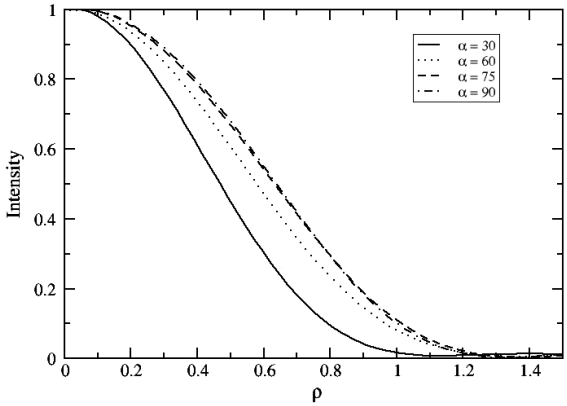

Figure 8. Intensity profile in a direction parallel to that of the transmission axis of the analyzer for different numerical apertures. The intensities are normalized to unity and the distance to the center of the image is scaled by the radius of the central peak predicted for scalar theory. The radius of the central peak of the diffraction pattern is broadened as the numerical aperture is increased.

while in vectorial theory they have just reached the resolution limit, as can be seen in figure 10. This indicates that. when the resolution of the system is studied under the scalar assumption, it is overestimated by approximately 10%.

5. Conclusions

We studied the diffraction pattern of a point source seen through a microscope considering both the scalar and vectorial diffraction theories. The point source was self-luminous, unpolarized, with dipolar electric moment randomly varying with time and no preferred direction in space. This object was modeled as a superposition of three uncorrelated orthogonal dipoles. The microscope was assumed to be free of aberrations, birefringence and polarization, and to fulfill the Abbe sine condition. We found that the size of the diffraction pattern predicted by vectorial theory is greater than that predicted

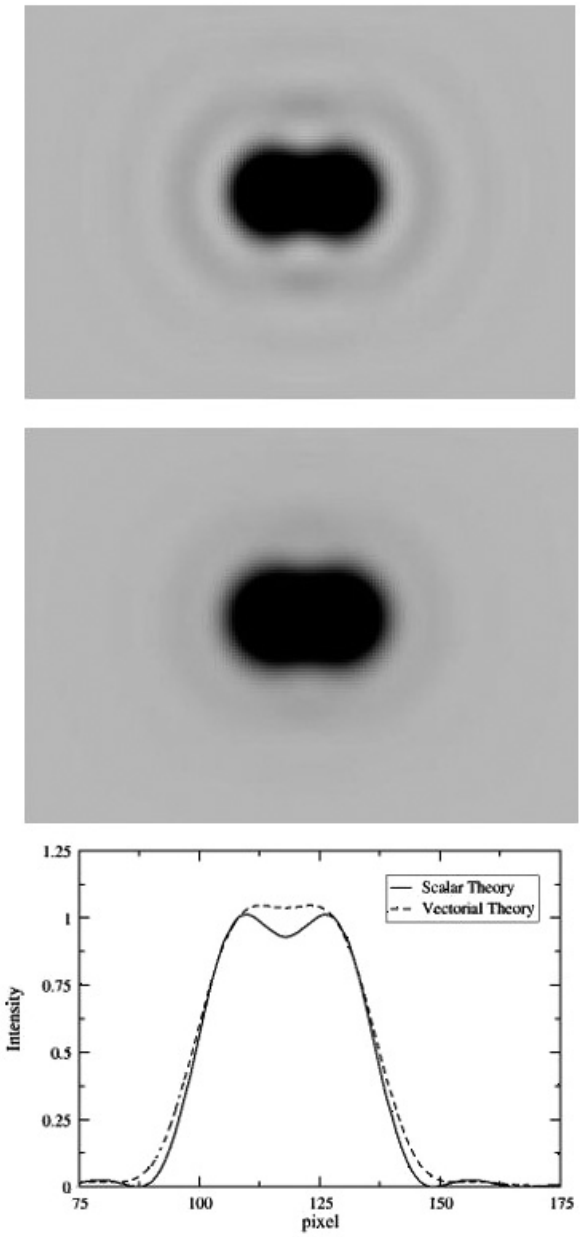

Figure 9. Results of simulating a two-point image separated a distance $d = 19$ pixels in the image. The upper image corresponds to considering scalar diffraction theory. The middle image corresponds to considering vectorial diffraction theory. The lower image corresponds to the intensity profiles for both cases. Notice that the image calculated according to scalar theory is just resolved while that corresponding to vectorial theory is not resolved.

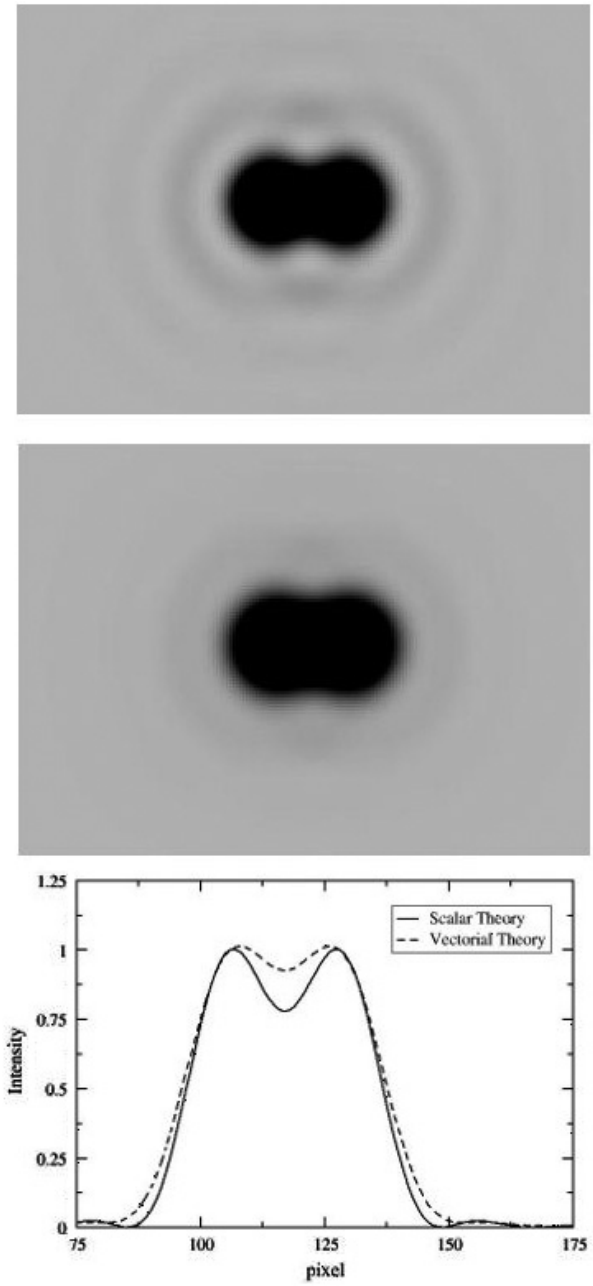

Figure 10. Results of simulating a two-point image separated a distance $d = 21$ pixels in the image. The upper image corresponds to considering scalar diffraction theory. The middle image corresponds to considering vectorial diffraction theory. The lower image corresponds to the intensity profiles for both cases. Notice that the image calculated according to scalar theory is well resolved while that corresponding to vectorial theory is just resolved.

by scalar diffraction theory. In the vectorial case, when an analyzer is placed behind the objective, the image shows an enlargement along the transmission axis of the analyzer. This is also observed in experimental diffraction patterns, indicating that our model is suitable for describing this phenomenon. Simulating a two-point image, we studied the resolution of the system, comparing scalar and vectorial diffraction theories. We found that minimal distance resolution for scalar theory is lower than that for the vectorial case. This implies that the resolution of the system under scalar assumptions is overestimated. In our case, for the specific parameters used in this simulation the overestimation amounts to as much as 10%.

Acknowledgments

We thank Drs Fornaro and González from the Instituto de Física y Matemática of the Universidad del Centro de la Provincia de Buenos Aires for the images. We also thank Dr Pellizza for his help. This work was supported by CONICET and a grant from the Universidad de Buenos Aires.

References

Jackson J D 1975 *Classical Electrodynamics* 2nd edn (New York: Wiley)

Richards B and Wolf E 1959 Electromagnetic diffraction in optical systems II. Structure of the image field in an aplanatic system *Proc. R. Soc.* A **253** 358–79

Sheppard C J R and Wilson T 1982 The image of a single point in microscopes of large numerical aperture *Proc. R. Soc.* A **379** 145–58

Simon M C, Simon J M and Garea M T 1987 Phase shift in dielectric reflection *Appl. Opt.* **26** 3871–7

Török P, Higdon P D and Wilson T 1997 On the general properties of polarised light conventional and confocal microscopes *Opt. Commun.* **148** 300–15

Wilson T, Juškaitis R and Higdon P 1997 The image of dielectric points scatterers in conventional and confocal polarisation microscopes *Opt. Commun.* **141** 298–313

Zhan Q 2009 Cylindrical vector beams: from mathematical concepts to applications *Adv. Opt. Photon.* **1** 1–57